

Improvement in asphalt binder rutting performance and fatigue life using electrospun polyacrylonitrile (PAN) nanofibers

Alberto Gaxiola^a, Alexandra Ossa^{b,*}, Laura González-Maturana^b, Omar Llanes-Cárdenas^c, M.J. Chinchillas-Chinchillas^d, Clemente G. Alvarado-Beltrán^a, Andrés Castro-Beltrán^{a,*}

^a Universidad Autónoma de Sinaloa (UAS)-Facultad de Ingeniería Mochis. Fuente de Poseidón, Los Mochis 81210, Mexico

^b Universidad Nacional Autónoma de México (UNAM)-Instituto de Ingeniería, Universidad 3000, Ciudad de México 04510, Mexico

^c Centro Interdisciplinario de Investigación para el Desarrollo Integral Regional Unidad Sinaloa, Instituto Politécnico Nacional (IPN), Sinaloa 81049, Mexico

^d Departamento de Ingeniería y Tecnología, Unidad regional Guasave, Universidad Autónoma de Occidente (UAdeO), Sinaloa 81048, Mexico

ARTICLE INFO

Keywords:

Electrospun nanofibers
Rutting resistance
Fatigue life

ABSTRACT

Recently, high aspect ratio materials like nanofibers with outstanding mechanical properties have been developed and used to improve the mechanical characteristics of construction materials. However, despite the excellent results obtained in asphalt binder modification, only a few types of polymeric nanofibers have been used for this purpose. In this sense, polyacrylonitrile has good thermal and mechanical characteristics to maintain the shape at the typical temperatures the asphalt is heated.

This study evaluates the effect of electrospun polyacrylonitrile (PAN) nanofibers on the rutting resistance and fatigue parameters of asphalt binders. For this, fibers with an average diameter of 1.3 μm were prepared and randomly dispersed into neat PG 64–22 asphalt binder. Subsequently, a dynamic shear rheometer (DSR) was used to determine $G^*/\sin \delta$, J_{nr} , $R_{3.2}$, and N_f .

In the range studied, $J_{nr_{3.2}}$ showed a reduction of up to 35%, and the elastic recovery increased up to 4.5 times compared to the reference material. It was observed that the PAN nanofibers increased the fatigue resistance of asphalt binder at temperatures when the material is predominantly viscoelastic. These results show a promising new application of PAN nanofibers to improve the performance of asphalt pavements.

1. Introduction

Asphalt concrete is a versatile construction material prepared with asphalt binder and mineral aggregate. It is flexible, impervious, and can withstand the loads imposed by road traffic. However, it can present problems such as moisture damage, rutting, thermal and fatigue cracking [1–3]. On the other hand, traffic conditions have provoked increasing loads, which demands better performance characteristics of the binders to minimize these problems [4–7]. For this, material modification has been an alternative, primarily with polymers. This procedure is performed when a material is incorporated into asphalt binder via mechanical mixing or chemical reactions [8,9]. However, high amounts of modifying agents are usually required to obtain satisfactory results, which can significantly increase costs [10–12]. In the paving industry, two types of polymers are primarily used: plastomers and elastomers. Plastomers generally consist of ethylene vinyl acetate (EVA) [11–13] copolymers, and the best-known thermoplastic elastomer is

styrene-butadiene-styrene (SBS) [14–16]. For this, 2–10% by weight polymer contents have been used to achieve adequate performance. However, other researchers reported that this content could attain a value of up to 25% in waterproofing membranes when the polymer is low-cost [13].

Recently, other alternatives for asphalt binder modification have been studied in which substantially lower amounts of modifying agents are used, i.e., nanomaterials [14]. These include nanofibers, generally defined as fibers with a diameter of less than one μm [15]. Because the diameter of the nanofibers is substantially smaller than the average asphalt film thickness in the mixtures (–8–10.5 μm) [16–19], they are considered a modifier. In contrast, regular fibers are another ingredient of the mixture and act as a reinforcement. For instance, Khattak et al. [20] used carbon nanofibers 60–150 nm in diameter and 30–100 μm in length to modify a neat asphalt binder. They determined that both rutting resistance and fatigue life improved after adding 2% nanofibers by weight. Yao et al. [21] improved rutting resistance by adding

* Corresponding authors.

E-mail addresses: aossal@ingen.unam.mx (A. Ossa), andres.castro@uas.edu.mx (A. Castro-Beltrán).

Table 1
Physical characteristics of the neat asphalt binder from the Mexican refinery of Tula.

Physical property and standard procedure	Result
Superpave designation, ASTM D6373-21a [29]	PG 64-22
Density, ASTM D70-18a [30]	1030 kg/m ³
Viscosity at 135 °C, ASTM D4402/D4402M-15 °C [31]	0.444 Pa.s
Viscosity at 165 °C, ASTM D4402/D4402M-15 [31]	0.118 Pa.s
Complex modulus at 64 °C, ASTM D7175 [32]	6707 Pa
Phase angle at 64 °C, ASTM D7175 [32]	78.5°

microfibers 3 mm in length and 18 μm in diameter, with 2% and 4% by weight. Arabani and Shabani [22] evaluated the effect of ceramic fibers with 2.5–3 μm in diameter and 20 mm in length on asphalt binder

modification. They found that the rutting resistance increased, although these fibers were not adequate under low-temperature conditions.

It is clear that fibrous materials improve the mechanical characteristics of asphalt binders. On the other hand, it is important to note that the greater the surface area of the material, the better the physical and mechanical interactions [23]. Therefore, nanofibers have been studied in the literature as an asphalt binder modifier, including cellulose and carbon nanofibers [24,25].

When exploring new applications of polymeric nanofibers in asphalt binder modification, it is essential to know the physical characteristics of the polymer in advance to optimize its performance with the least amount of fibers. PAN exhibits good thermal and mechanical characteristics for use as nanofiber in asphalt binder modification because the melting temperature is above the typical temperatures at which asphalt

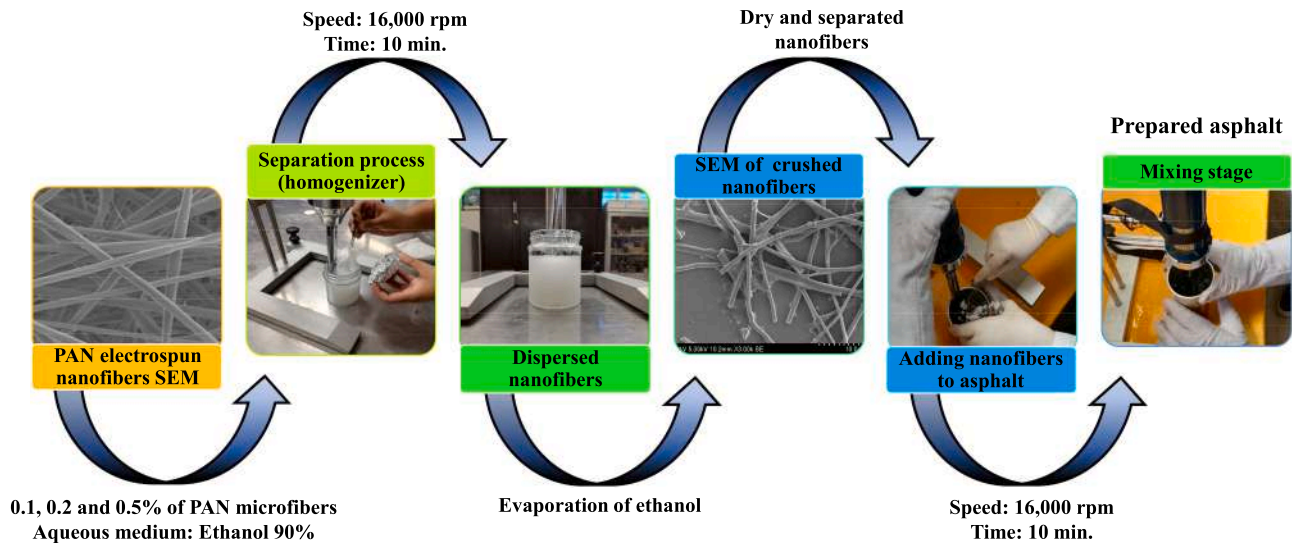


Fig. 1. Dispersion of PAN nanofibers into asphalt binder.

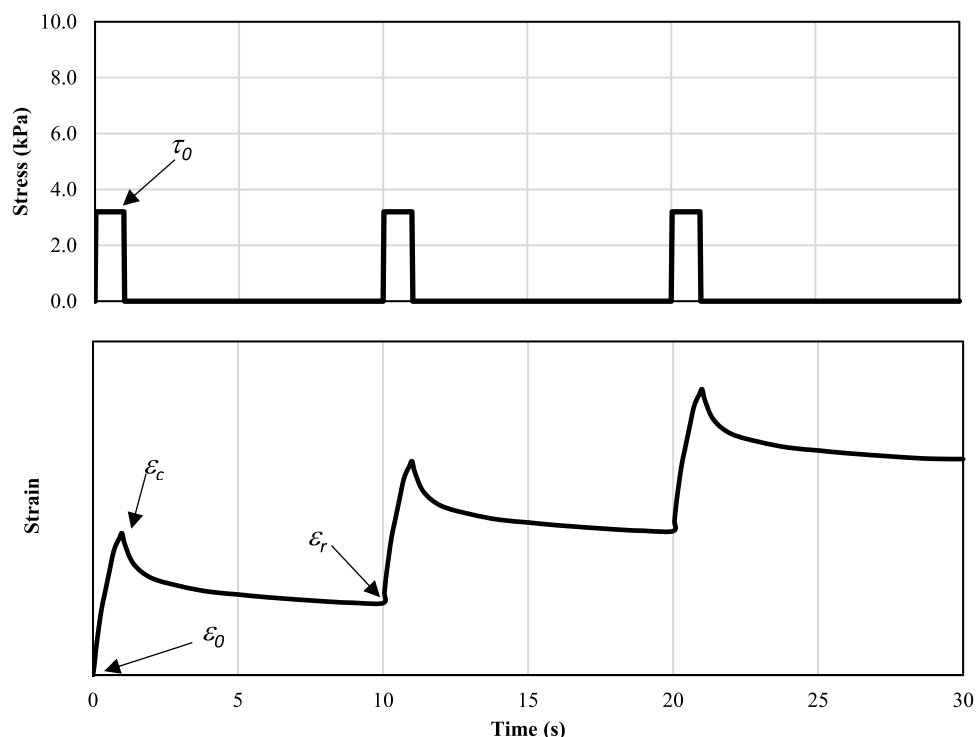


Fig. 2. Stress and strain patterns of asphalt binder in MSCR test.

Table 2
Equations of the LAS method [47].

Equation	Symbol and description
$N_f = A(\gamma_{max})^{-B}$	N_f = Fatigue performance parameter
$A = \frac{f(D_f)^k}{k(\pi C_1 C_2)^a}$	A, B = Parameters for the asphalt binder fatigue performance
$k = 1 + (1 - C_2)\alpha$	γ_{max} = maximum strain, %
$D_f = \left(\frac{C_0 - C_p}{C_1}\right)^{1/C_2}$	f = loading frequency, Hz
$C(t) = \frac{ G^* (t)}{ G^* _{initial}}$	$D_f = D(t)$ at peak stress
$C(t) = C_0 - C_1(D)^{C_2}$	C_1, C_2 = curve-fit coefficients
	$C_p = C$ at peak stress
	$C_0 = 1$
$D(t) =$	t = testing time, s
	$D(t)$ = damage accumulation
$\sum_{i=1}^N [\pi \gamma_0^2 (C_{i-1} - C_i)]^{1+\alpha} (t_i - t_{i-1})^{1+\alpha}$	α, m, b = best-fit straight-line parameters
$\log G^*(\omega) = m \log \omega + b$	ω = angular frequency, rad/s
$\alpha = 1/m$	$ G^*(\omega) $ = dynamic modulus, MPa
$G^*(\omega) = G^*(\omega) \times \cos \delta(\omega)$	$\delta(\omega)$ = phase angle, rad
	$G^*(\omega)$ = storage modulus, MPa

is mixed and compacted in the field [26,27].

This study presents a new application of PAN nanofibers to asphalt binder modification. These nanostructures were prepared by the electrospinning technique (electrospun nanofibers) and later dispersed, in contents of 0.0, 0.1, 0.2, and 0.5 wt.%, into a material that did not comply with the specification for asphalt binders graded using multiple stress creep recovery (MSCR) [28]. Subsequently, the performance parameters $G^*/\sin \delta$, creep compliance, elastic recovery, and the number of cycles at failure were evaluated to the PAN nanofibers modified asphalt binder (PNMAB). The preparation satisfied the requirements for standard traffic after adding only 0.2% nanofibers, while the fatigue resistance also improved.

2. Experimental

2.1. Materials

To synthesize the nanofibers, PAN (Mw=150,000 g/mol, Sigma Aldrich) and N,N-dimethylformamide (DMF, 99.85% purity, CTR Scientific) were used. Ethanol (99% purity) was used to disperse the nanofibers into a liquid medium and cut them. The asphalt binder was PG 64–22 sourced from the Tula refinery in Mexico. The physical characteristics of the binder are outlined in Table 1.

2.2. Preparation and dispersion of the PAN nanofibers

PAN nanofibers were synthesized using the electrospinning method

described by Chinchillas et al. [26]. To obtain short and randomly oriented nanofibers from the continuous material, they were dispersed into a liquid medium. Ethanol was used for this purpose because it does not dissolve PAN and it has a high evaporation ratio.

First, the PAN nanofibers (2 g) were weighed and then added to a beaker. Subsequently, ethanol (40 ml) was poured, and the dispersion process was carried out using a high shear device (DLAB D-500) at 10,000 rpm for 10 min. Thereafter, ethanol was allowed to evaporate at room temperature and pressure for approximately 12 h. The next step involved the addition of PAN nanofibers (short and dry) to the asphalt binder. In this process, the asphalt binder was heated to 160 °C to reduce its viscosity, and the nanofibers were added to the liquid asphalt binder.

Finally, the nanofibers were dispersed into the asphalt binder using the same homogenizer previously used at the same speed for 4 min. The nanofiber contents used to prepare the mixtures were 0.1, 0.2, and 0.5% wt, similar to those used by Chinchillas in investigations carried out with these nanofibers in cementitious materials [33,34]. Fig. 1 graphically shows the process of addition and dispersion of PAN nanofibers to the asphalt binder. Initially, the process of dispersing and cutting the nanofibers was attempted directly in liquid asphalt binder at 160 °C. However, the viscosity of the asphalt binder is still high at this temperature compared to the viscosity of ethanol; therefore, the high shear device was unable to cut the nanofibers and only caused them to coil on its rod.

2.3. Evaluation of the rutting parameters

In this study, the rutting resistance was investigated by simulating the conditions of the material during asphalt mixture production and laydown, that is, after short-term aging. In this sense, the $G^*/\sin \delta$ and MSCR values were obtained after running the rolling thin-film oven (RTFO) tests on asphalt binders according to the AASHTO T 240 test method [35].

2.3.1. $G^*/\sin \delta$

Report SHRP-A-410 [36] indicates that the performance grade (PG)

Table 3
Physicochemical properties of PAN nanofibers.

Property	Result
Color	White
Average diameter	1.3 μm
Morphology	Homogeneous
Hardness	0.49 GPa
Elastic modulus	2.49 GPa
Glass transition point	107 °C
Melting point	287 °C

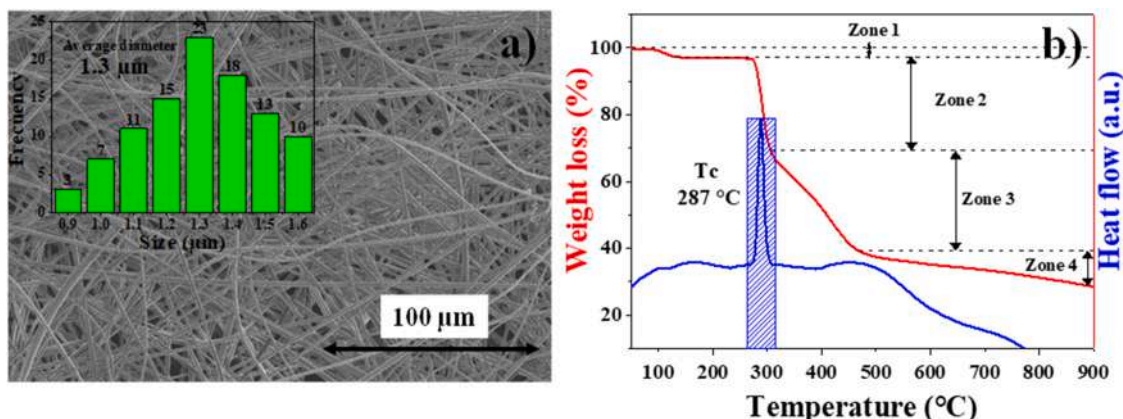


Fig. 3. Micrographs and thermogravimetric analysis (TGA) of PAN nanofibers.

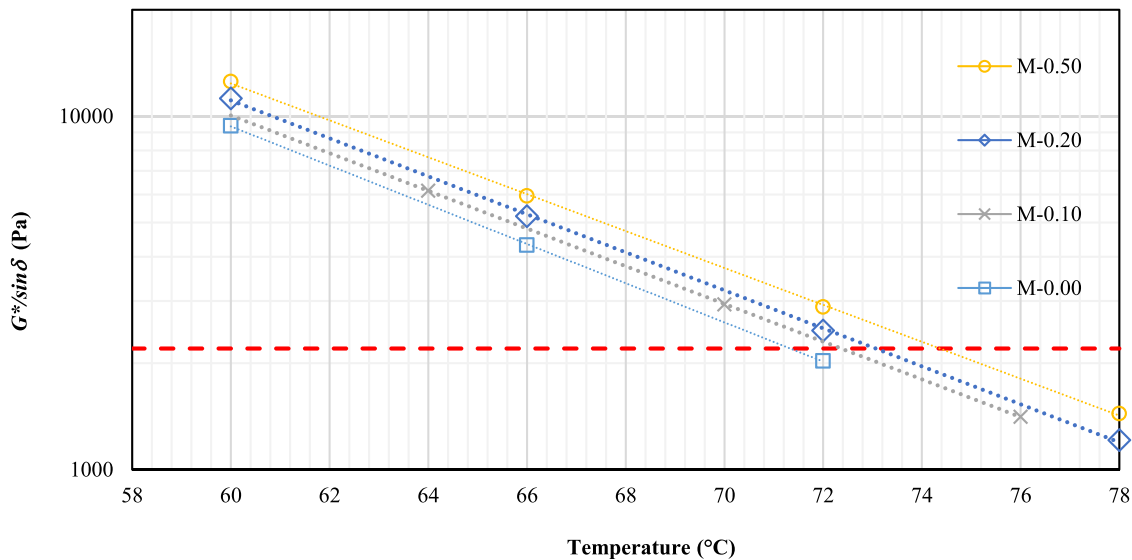


Fig. 4. $G^*/\sin \delta$ as a function of temperature for PNMA.

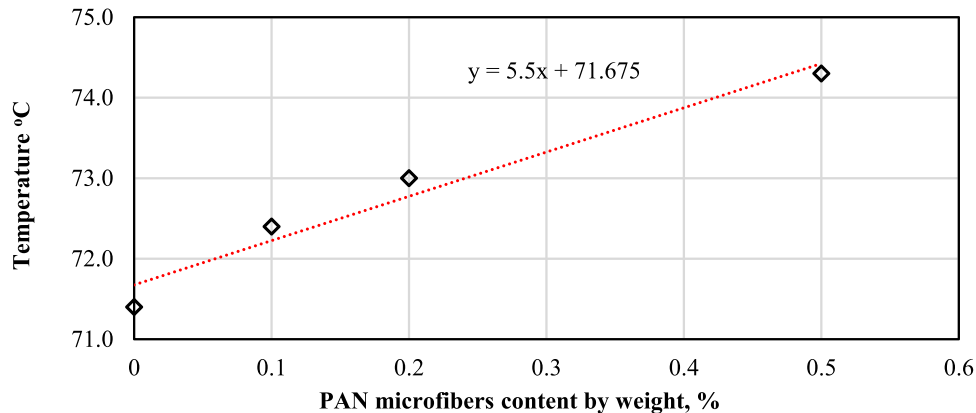


Fig. 5. Specification of $G^*/\sin \delta$ (2.2 kPa) as a function of nanofibers content.

of an asphalt binder is designated as PG XX-YY, where XX is the maximum design temperature and YY is the minimum, in °C. Both denote the average temperatures of seven consecutive days with the highest and lowest values, respectively. XX was established using SUPERPAVE based on the rutting resistance of the asphalt binder.

The ASTM D6373 specification designates grades from PG 46-YY to PG 82-YY [37]. For this purpose, the SUPERPAVE methodology uses the maximum dissipated energy per loading cycle, W_i . The formula for this calculation is expressed in Eq. (1), where τ_0 is the maximum shear stress applied, G^* is the complex modulus, and δ is the phase angle. The term $G^*/\sin \delta$, established in the ASTM and AASHTO standards, originates from Eq. (1) [38–40].

$$W_i = \pi \tau_0^2 \frac{1}{G^*/\sin \delta} \quad (1)$$

$G^*/\sin \delta$ is among the first parameters used in a DSR to characterize rutting resistance [41].

In this study, to obtain G^* and δ , the procedure described in AASHTO T315 was performed using DSR [40]. Specimens with a diameter of 25 mm and a height of 1 mm were prepared using a silicone mold. Further, using DSR, strain-controlled sinusoidal loads were applied to the samples. The angular frequency and strain were 10 rad/s (1.59 Hz) and 10%, respectively.

The temperature was set at 60 °C before performing the DSR test on each specimen. The process of loading and data recording was repeated

with temperature increments of 6 °C. The test was stopped when $G^*/\sin \delta$ was less than 2.2 kPa. At this stress, the asphalt binder no longer exhibited good performance with the temperature applied to the specimens aged by RTFO.

2.3.2. MSCR

Dongré and D’Angelo reported results measured on test roads, where the rut depth was not consistent with the expected values according to $G^*/\sin \delta$. For instance, they analyzed the measurements obtained from two test roads, one composed of unmodified PG 67–22 and another of polymer-modified PG 63–22 asphalt binder. In contrast to expectations, pavements made with PG 67–22 asphalt binder exhibited a 15 mm rut depth, and those with PG 63–22 exhibited no rut [42].

In 2003, Delgado et al. proposed to change $G^*/\sin \delta$ for another parameter named *viscous component of the creep stiffness* G_v , as it showed a good correlation with rutting [43]. D’Angelo correlated the results of multi-stress creep recovery (MSCR) with rut depth. Subsequently, the MSCR results began to be considered as a replacement of the current $G^*/\sin \delta$ by J_{nr} , which correlates much better with rut depth, with R^2 values of 0.8167 and 0.223 [44].

Before conducting the MSCR tests, the short-term aging process of asphalt binder was simulated using an RTFO [45]. A silicone mold was used to prepare specimens with a diameter of 25 mm and a height of 2 mm. Two stress levels and two temperatures were used to determine the elastic response and creep recovery of asphalt binder; that is, stresses of

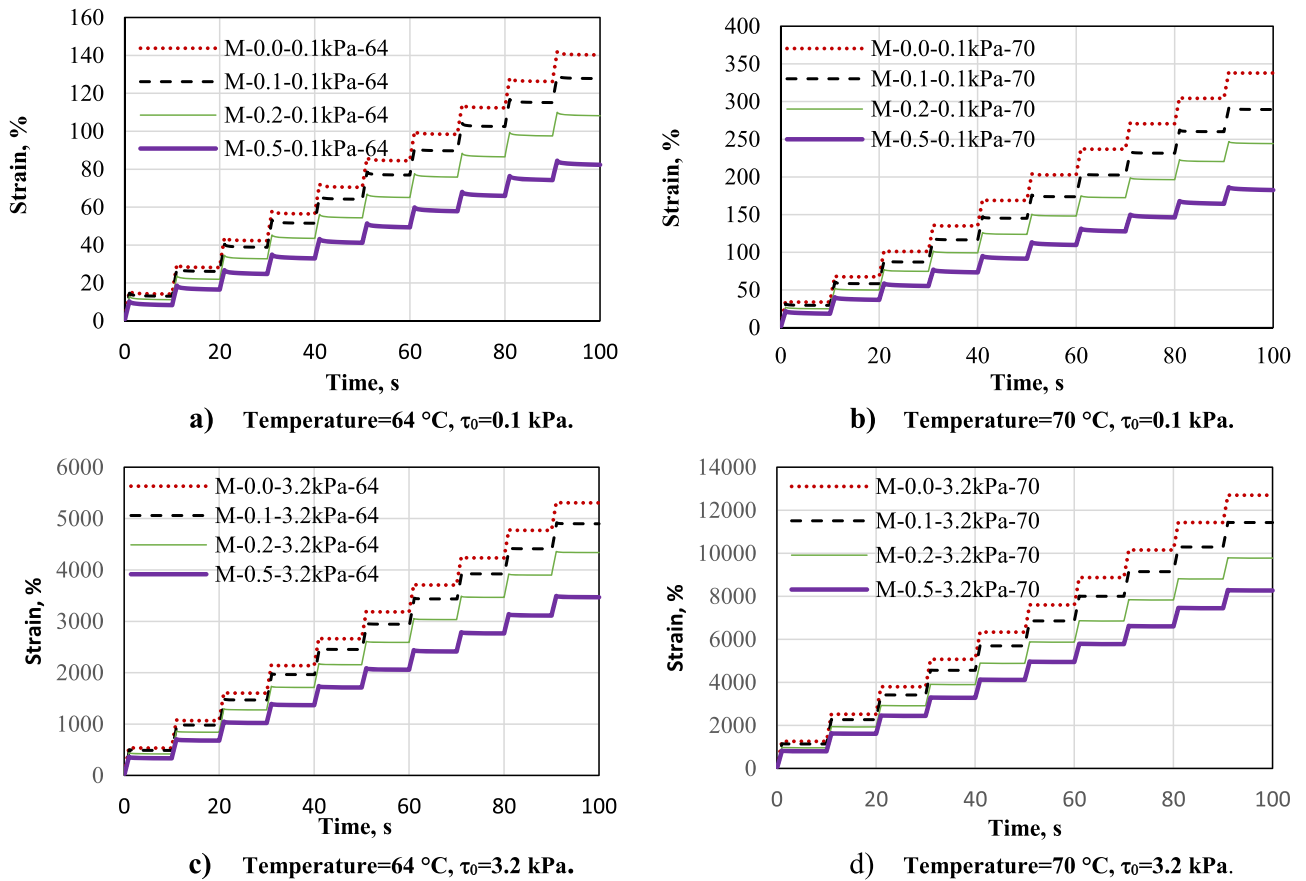


Fig. 6. Results of multiple stress creep recovery (MSCR) tests.

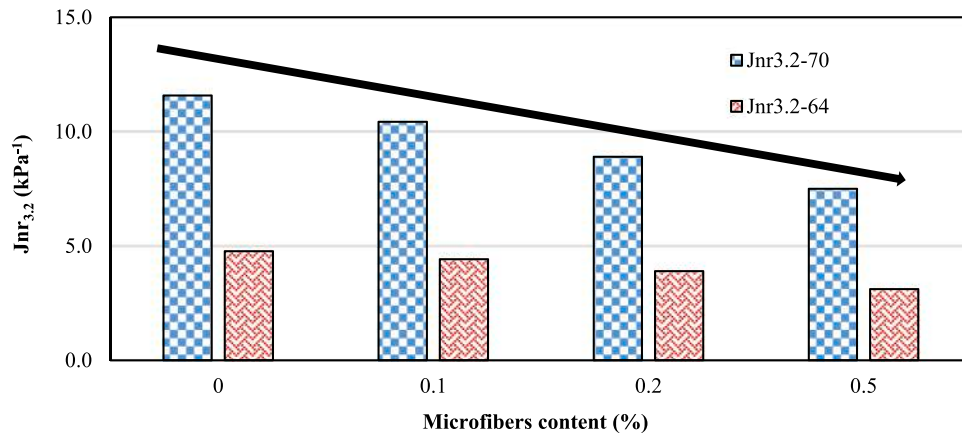


Fig. 7. Creep compliance as a function of the content of PAN nanofibers in asphalt binder.

0.1 and 3.2 kPa, and temperatures 64 and 70 °C. These stresses were maintained for 1.0 s and then removed for 9.0 s. In each test, 10 cycles were applied for 100 s of total [46]. Fig. 2 shows a graph of the applied and recorded stress and strain patterns.

The initial strain was recorded at the beginning of the creep portion (ϵ_0), at the end of the creep portion (after 1 s, ϵ_c), and at end of the 10 s period of each cycle (ϵ_r). The portion of recovered strain is denoted by $\epsilon_{10} = \epsilon_r - \epsilon_0$.

$$\epsilon_r = \frac{\epsilon_1 - \epsilon_{10}}{\epsilon_1} \times 100 \quad (2)$$

Following 10 cycles of stress τ_0 , the elastic recovery (R) and creep compliance (J_{nr}) were calculated using Eqs. (3) and (4), respectively.

$$R = \frac{\sum_{N=1}^{10} \epsilon_r}{10} \quad (3)$$

$$J_{nr} = \frac{\sum_{N=1}^{10} (\epsilon_{10} / \tau_0)}{10} \quad (4)$$

2.4. Evaluation of the fatigue life

To evaluate the fatigue life of neat asphalt binder and of the asphalt binder modified with PAN nanofibers after RTFO and pressure aging vessel (PAV) aging, linear amplitude sweep (LAS) was used according to AASHTO TP 101[47] through a DSR using binder samples 8 mm in

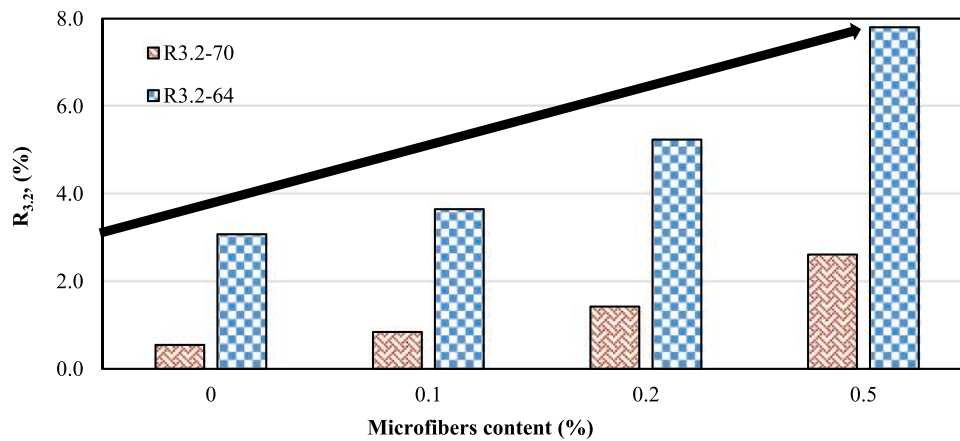


Fig. 8. Elastic recovery as a function of PAN nanofibers in asphalt.

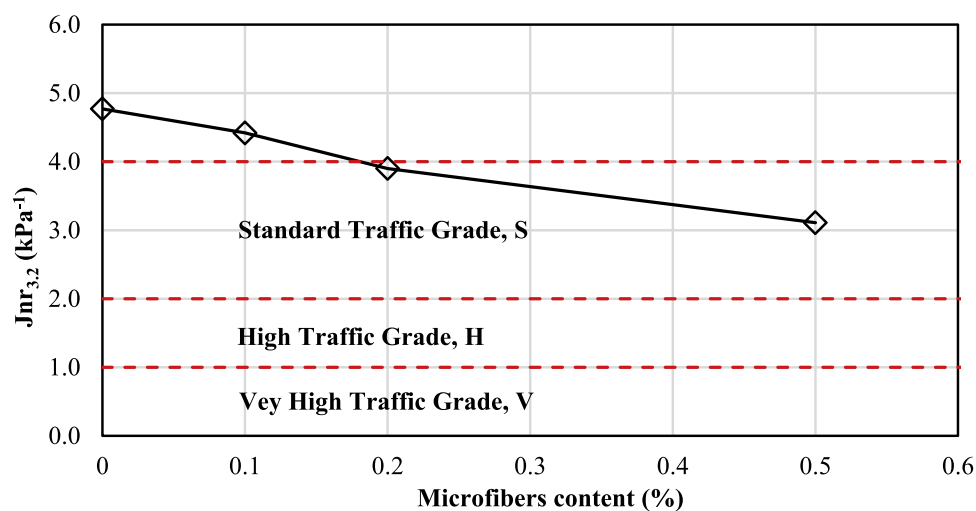


Fig. 9. Traffic grade specification and Creep compliance of PNMA.

diameter.

In these tests, a frequency sweep was carried out from 0.2 to 30 Hz at a strain of 0.1% and later an amplitude sweep from 0 to 30%, keeping the frequency constant at 10 Hz. Finally, the coefficients A and B were obtained to determine the fatigue parameter, N_f , using the equations of Table 2.

Regarding the temperatures at which the fatigue life of the asphalt binder is evaluated, Kuchiishi et al. [48] discussed that the range most used in different investigations lay between 10 and 30 °C. In this study, the test temperatures started from 10 °C and increased until a change in the asphalt binder response was observed, as detailed in the next section. Thus, the test temperatures were 10, 20, 25, and 40 °C.

3. Results and discussion

3.1. Characterization of the PAN nanofibers

The PAN nanofiber morphology was analyzed employing scanning electron microscopy. The membrane-shaped nanofibers are shown in Fig. 3. The observed morphology was uniform, continuous, unattached, and with diameter ranging from 0.9 to 1.6 μm (1.3 μm average).

Furthermore, the thermal properties of the PAN nanofibers were evaluated using the thermogravimetric analyzer SBT model U600 in a nitrogen environment with temperature increments of 10 °C/min up to 800 °C. The results obtained indicate the desorption of water up to 120 °C (Zone 1), a negligible weight loss as a product of the cyclization

process at a temperature of 120 to 280 °C (Zone 2) [49], a weight loss that reflects a dehydrogenation (Zone 3) [50], and a final stage that exhibits the degradation of the material in pure carbon structures (Zone 4). The greatest weight loss was observed at approximately 275 °C, which corresponds to the melting point (T_m) of PAN. These results are consistent with other investigations found in the literature [51] and demonstrate the feasibility of using PAN nanofibers to reinforce and improve asphalt concrete because mixing and compaction temperatures of asphalt usually do not exceed 185 °C, even on modified asphalt binders [52,53].

The cylindrical structure of the material is maintained for the temperatures mentioned above and up to almost 300 °C of the melting point; that is, it is well above the mixing and compaction temperatures of asphalt concrete. Finally, Table 3 presents some of the physicochemical properties of the PAN nanofibers used in this research.

3.2. Effect of the PAN nanofibers on the rutting response

It is evident that the values of $G^*/\sin \delta$ shown in Fig. 4 tend to increase as a function of the PAN nanofiber content. To measure the improvement in the rutting resistance induced by these additions, it is possible to use the methods ASTM D6373 and AASHTO M320 [38,39], where a threshold of 2.2 kPa was established to determine the performance grade (PG) of the asphalt binder after short-term aging using an RTFO described in AASHTO T240 and ASTM D2872 [35,45].

Fig. 5 shows the line of best fit for the temperature when 2.2 kPa of

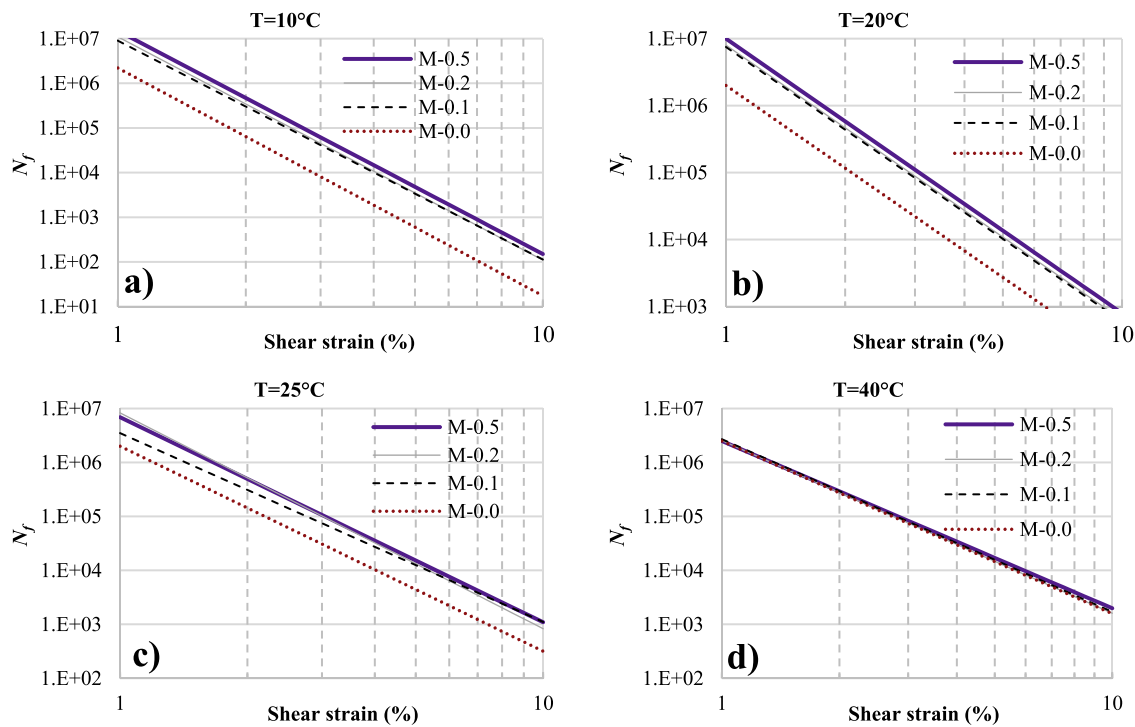


Fig. 10. Fatigue parameter N_f versus applied shear strain for PNMAb.

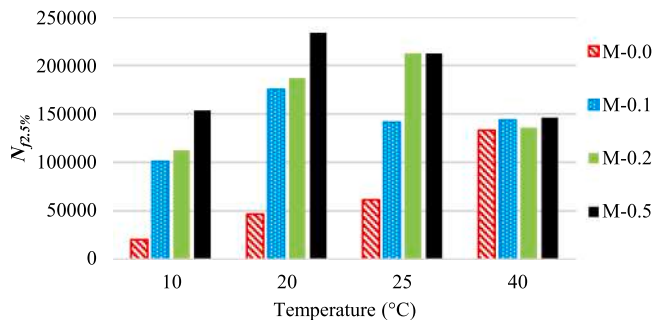


Fig. 11. Allowable fatigue life at 2.5% strain.

$G^*/\sin \delta$ were obtained as a function of PAN nanofibers content. This line presents a slope of $5.5 \text{ }^\circ\text{C}/\%$ in the range of nanofiber content analyzed.

All measurements of rutting resistance made on the PNMAb showed an improvement. For instance, the test conducted at $64 \text{ }^\circ\text{C}$ and 0.1 kPa yielded a final cumulative strain of 140.2% for the neat asphalt binder, whereas the asphalt binder with 0.5% of nanofiber content reduced this cumulative strain up to 82.3% (see Fig. 6a). Moreover, this behavior was consistent for all MSCR tests. Figs. 6a to 6d show these results for temperatures of 64 and $70 \text{ }^\circ\text{C}$, and the two stress levels established by AASHTO TP70 [46].

Fig. 7 shows the manner in which the creep compliance tends to decrease with an increase in the nanofiber content. For the temperature of $70 \text{ }^\circ\text{C}$, $J_{nr,3.2}$ decreased from 11.6 to 7.6 kPa^{-1} , indicating a reduction of 35% . In a similar manner, $J_{nr,3.2}$ at $64 \text{ }^\circ\text{C}$, passed from 4.8 kPa^{-1} for neat asphalt binder to 3.1 kPa^{-1} upon addition of a content with 0.5% by weight of binder. Compared to the neat asphalt, the elastic recovery increased 2.5 times and 4.7 times for the temperatures of 64 and $70 \text{ }^\circ\text{C}$, respectively (see Fig. 8).

The results demonstrate a significant enhancement in the rutting resistance of asphalt binder through the incorporation of PAN nanofibers. This improvement can be attributed to the high surface area of these nanofibers, which promotes strong interactions between the

nanofiber and the matrix. As a result, the asphalt binder exhibits an elastic recovery effect that consistently displays a positive trend within the explored range.

The neat asphalt binder used in this investigation did not satisfy the specification AASHTO MP19–10 for any of the traffic levels [28]. The standard traffic level (S) specifies that the asphalt binder must have a $J_{nr,3.2}$ of 4 kPa^{-1} or less, while this asphalt binder exhibited 4.77 kPa^{-1} . Moreover, this parameter showed a consistent tendency to decrease with an increase in the PAN nanofiber content, and with only 0.2% by weight, the parameter complied with the specification (See Fig. 9).

3.3. Fatigue life

For the temperatures of 10 , 20 and $25 \text{ }^\circ\text{C}$, the fatigue life of the asphalt binder increased as a function of the PAN nanofibers content, i. e., the position of all the curves in Fig. 10 was above than those of M-0.0 specimens. However, when analyzing Fig. 10d, it is clear that PAN nanofibers have no effect on fatigue life when applying a temperature of $40 \text{ }^\circ\text{C}$.

There are different criteria to compare the fatigue life of asphalt binder from LAS test results, among which the stored pseudostrain energy (PSE) [54], the fatigue area factor (FAF), and N_f at 2.5% strain ($N_{f2.5\%}$) stand out [48,55,56]. The latter has gained popularity among researchers because it is considered an adequate deformation to compare the fatigue life of asphalt binders [48,57–59]. The results of $N_{f2.5\%}$ of the asphalt binder evaluated in this study are shown in Fig. 11. The analyses began with a temperature of $10 \text{ }^\circ\text{C}$, where $N_{f2.5\%}$ was $20,000$ for the neat asphalt binder and gradually increased to $150,000$ for the asphalt binder modified with 0.5% of PAN nanofibers. A similar effect was observed with 20 and $25 \text{ }^\circ\text{C}$ of temperatures. However, when analyzing the results obtained at $40 \text{ }^\circ\text{C}$, no significant change was observed in the fatigue life of the neat asphalt binder compared to the PNMAb, regardless of the content used. Next, we propose a mechanism explaining why this occurs in asphalt binder at this temperature level.

A pure elastic material shows a 0° phase angle, while the phase angle of a pure viscous material is 90° . In this sense, some authors classify the mechanical response of asphalt binder in three viscoelastic ranges:

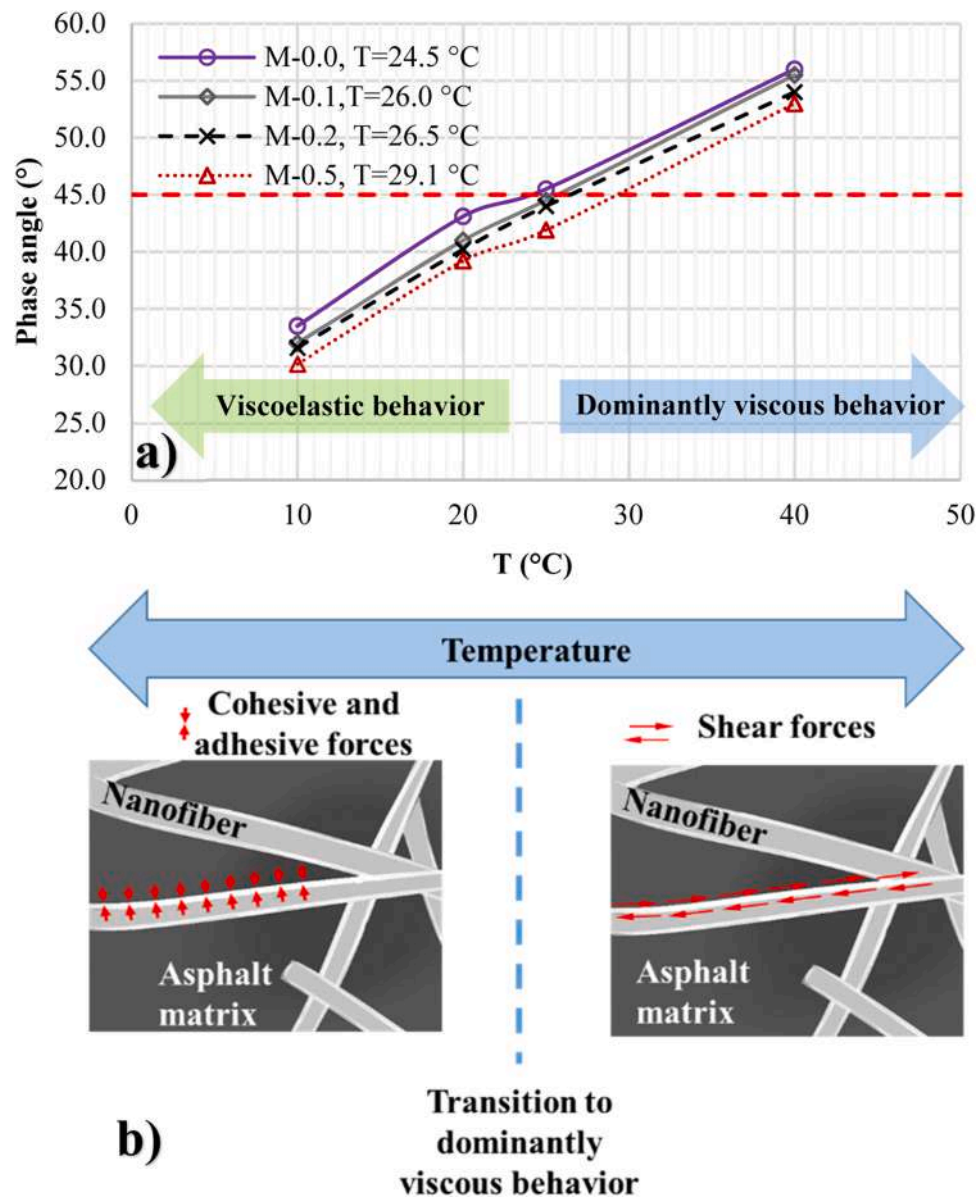


Fig. 12. (a) Phase angle of PNMAb as a function of temperature and (b) the mechanism of influence of cohesive and adhesive forces in fatigue life.

dominantly elastic where the phase angle is less than 5° , viscoelastic with phase angles between 5° and 45° , and dominantly viscous for phase angles higher than 45° [60,61].

With the asphalt binders prepared with the nanofiber contents of this study, we can observe in Fig. 12a that the threshold that separates the viscoelastic from the dominantly viscous behavior ranges from 24.5 to 29.1 °C, i.e., for temperatures higher than these, the dominant behavior was viscous. At working temperatures of asphalt binder, cohesion and adhesion decreases as temperature increases [62], and these forces directly influence fatigue resistance [63]. This is explained in Fig. 12b, where we can observe that when the asphalt binder was tested at temperatures below this threshold, the cohesive and adhesive forces dominated, and the PAN nanofibers had important effect on the fatigue resistance of asphalt binder. On the other hand, when the asphalt binder was tested at a higher temperature, the forces that dominated were the shear forces, and the fibers did not provide more fatigue life (See Fig. 12).

4. Conclusions

PAN nanofibers were electrospun and added to neat Mexican asphalt in small amounts compared to the typical polymer contents added with other techniques, although the performance achieved was satisfactory. In the range of 0–0.5% of PAN nanofibers by weight, a steady increase in the parameter established by SUPERPAVE to characterize rutting resistance was recorded. The rate of change in temperature as a function of nanofibers content, when $G^*/\sin \delta$ reached 2.2 kPa, was $5.5^\circ\text{C}/\%$.

Further, the results of the MSCR tests showed better mechanical characteristics of the asphalt binder, that is, creep compliance decreased and elastic recovery increased. Specifically, the neat asphalt binder did not satisfy the requirements of standard grade, but when containing only 0.2% nanofibers by weight of asphalt binder, it did.

PAN nanofibers have an important effect on the fatigue resistance of PNMAb at temperatures when the viscoelastic effect domains. However, when temperature increases to a dominantly viscous behavior, the PAN nanofibers do not affect fatigue parameter N_f .

These results present PAN nanofibers as an alternative for improving the rheological characteristics of asphalt binders.

Declaration of Competing Interest

The authors declare that they have no known competing financial interests or personal relationships that could have appeared to influence the work reported in this paper.

Data availability

Data will be made available on request.

Acknowledgments

The authors wish to thank DGIP-UAS PROFAPI 2022/PRO-A8-005, and CONAHCYT for the support received in this investigation.

References

- I. Boz, G.P. Coffey, J. Habbouche, S.D. Diefenderfer, O.E. Ozbulut, A critical review of monotonic loading tests to evaluate rutting potential of asphalt mixtures, *Constr. Build. Mater.* 335 (2022), 127484, <https://doi.org/10.1016/j.conbuildmat.2022.127484>, February.
- J.W. dos S. Ferreira, J.F.R. Marroquin, J.F. Felix, M.M. Farias, M.D.T. Casagrande, The feasibility of recycled micro polyethylene terephthalate (PET) replacing natural sand in hot-mix asphalt, *Constr. Build. Mater.* 330 (2022), <https://doi.org/10.1016/j.conbuildmat.2022.127276>, December 2021.
- H. Zhang, H. Liu, W. You, Microstructural behavior of the low-temperature cracking and self-healing of asphalt mixtures based on the discrete element method, *Mater. Struct. Constr.* 55 (1) (2022) 1–17, <https://doi.org/10.1617/s11527-021-01876-7>.
- K. Yang, et al., Functional adjustment and cyclic application of Fe–Mn bimetal composite for Sb(V) removal: transformation of iron oxides forms and a stable regeneration method, *J. Clean. Prod.* 266 (2020), 122007, <https://doi.org/10.1016/j.jclepro.2020.122007>.
- B. Singh, P. Kumar, Effect of polymer modification on the ageing properties of asphalt binders: chemical and morphological investigation, *Constr. Build. Mater.* 205 (2019) 633–641, <https://doi.org/10.1016/j.conbuildmat.2019.02.050>.
- H.B. Birgin, A. D'Alessandro, A. Corradini, S. Laflamme, F. Ubertini, Self-sensing asphalt composite with carbon microfibers for smart weigh-in-motion, *Mater. Struct. Mater. Constr.* 55 (5) (2022), <https://doi.org/10.1617/s11527-022-01978-w>.
- G. García, N. Corte, Experimental study on an *in situ* concrete block pavement under heavy traffic loads, *Int. J. Pavement Eng.* 23 (10) (2022) 3467–3480, <https://doi.org/10.1080/10298436.2021.1902523>.
- H. Yu, et al., Modification effects of multi-walled carbon nanotubes on the mechanical and rheological properties of epoxy asphalt, *Constr. Build. Mater.* 369 (2023), 130154, <https://doi.org/10.1016/j.conbuildmat.2022.130154>, August 2022.
- Y. Deng, M. Hu, L. Xu, S. Ling, H. Ni, D. Sun, Dual roles played by manganese dioxide filler in asphalt pavement material: chemical modification and healing improvement, *Constr. Build. Mater.* 345 (2022), 128371, <https://doi.org/10.1016/j.conbuildmat.2022.128371>, May.
- K.L. Roja, A. Rehman, M. Ouederni, S.K. Krishnamoorthy, A. Abdala, E. Masad, Influence of polymer structure and amount on microstructure and properties of polyethylene-modified asphalt binders, *Mater. Struct. Mater. Constr.* 54 (2) (2021) 1–17, <https://doi.org/10.1617/s11527-021-01683-0>.
- F. Cardone, S. Spadoni, G. Ferrotti, F. Canestrari, Asphalt mixture modification with a plastomeric compound containing recycled plastic: laboratory and field investigation, *Mater. Struct. Mater. Constr.* 55 (3) (2022), <https://doi.org/10.1617/s11527-022-01954-4>.
- M.A. Dalhat, K. Al-adham, Review on laboratory preparation processes of polymer modified asphalt binder, *J. Traffic Transp. Eng. Engl. Ed.* (2023), <https://doi.org/10.1016/j.jtte.2023.01.002>.
- C. Giavarini, P. De Filippis, M.L. Santarelli, M. Scarsella, Production of stable polypropylene-modified bitumens, *Fuel* 75 (6) (1996) 681–686, [https://doi.org/10.1016/0016-2361\(95\)00312-6](https://doi.org/10.1016/0016-2361(95)00312-6).
- K. Debbarma, B. Debnath, P.P. Sarkar, A comprehensive review on the usage of nanomaterials in asphalt mixes, *Constr. Build. Mater.* 361 (2022), 129634, <https://doi.org/10.1016/j.conbuildmat.2022.129634>, November.
- S. Kailasa, M.S.B. Reddy, M.R. Maurya, B.G. Rani, K.V. Rao, K.K. Sadasivuni, Electrospun nanofibers: materials, synthesis parameters, and their role in sensing applications, *Macromol. Mater. Eng.* 306 (11) (2021) 1–36, <https://doi.org/10.1002/mame.202100410>.
- X. Li, C.R. Williams, M.O. Marasteanu, T.R. Clyne, E. Johnson, Investigation of In-Place asphalt film thickness and performance of hot-mix asphalt mixtures, *J. Mater. Civ. Eng.* 21 (6) (2009) 262–270, [https://doi.org/10.1061/\(ASCE\)0899-1561\(2009\)21:6\(262\)](https://doi.org/10.1061/(ASCE)0899-1561(2009)21:6(262)).
- A. Gaxiola, A. Ossa, Hydraulic, volumetric, and mechanical approach in asphalt mixture design for impervious barriers, *J. Mater. Civ. Eng.* 31 (2) (2019) 1–10, [https://doi.org/10.1061/\(ASCE\)MT.1943-5533.0002613](https://doi.org/10.1061/(ASCE)MT.1943-5533.0002613).
- P.S. Kandhal, S. Chakraborty, Effect of asphalt film thickness on short- and long-term aging of asphalt paving mixtures, *Transp. Res. Rec.* (1535) (1996) 83–90, <https://doi.org/10.3141/1535-11>.
- B. Sengoz, E. Agar, Effect of asphalt film thickness on the moisture sensitivity characteristics of hot-mix asphalt, *Build. Environ.* 42 (10) (2007) 3621–3628, <https://doi.org/10.1016/j.buildenv.2006.10.006>.
- M.J. Khattak, A. Khattab, H.R. Rizvi, P. Zhang, The impact of carbon nano-fiber modification on asphalt binder rheology, *Constr. Build. Mater.* (2012), <https://doi.org/10.1016/j.conbuildmat.2011.12.022>.
- H. Yao, et al., Rheological properties and chemical analysis of nanoclay and carbon microfiber modified asphalt with Fourier transform infrared spectroscopy, *Constr. Build. Mater.* 38 (2013) 327–337, <https://doi.org/10.1016/j.conbuildmat.2012.08.004>.
- M. Arabani, A. Shabani, Evaluation of the ceramic fiber modified asphalt binder, *Constr. Build. Mater.* 205 (2019) 377–386, <https://doi.org/10.1016/j.conbuildmat.2019.02.037>.
- M.S. Eisa, A. Mohamady, M.E. Basiouny, A. Abdulhamid, J.R. Kim, Mechanical properties of asphalt concrete modified with carbon nanotubes (CNTs), *Case Stud. Constr. Mater.* 16 (2022) e00930, <https://doi.org/10.1016/j.cscm.2022.e00930>, February.
- M.J. Khattak, A. Khattab, H.R. Rizvi, Mechanistic characteristics of asphalt binder and asphalt matrix modified with nano-fibers, *Geo-Frontiers 2011 Adv. Geotech. Eng.* 4 (2011) 4812–4822, [https://doi.org/10.1061/41165\(397\)492](https://doi.org/10.1061/41165(397)492).
- R. Ghabchi, M.P. Pereira Castro, Effect of laboratory-produced cellulose nanofiber as an additive on performance of asphalt binders and mixes, *Constr. Build. Mater.* 286 (2021), 122922, <https://doi.org/10.1016/j.conbuildmat.2021.122922>.
- M.J. Chinchillas-Chinchillas, et al., Evaluation of the mechanical properties, durability and drying shrinkage of the mortar reinforced with polyacrylonitrile microfibers, *Constr. Build. Mater.* (210) (2019) 32–39, <https://doi.org/10.1016/j.conbuildmat.2019.03.178>.
- M. Chinchillas-Chinchillas, et al., Synthesis of recycled poly(ethylene terephthalate)/Polyacrylonitrile/styrene composite nanofibers by electrospinning and their mechanical properties evaluation, *J. Polym. Environ.* 27 (2019), <https://doi.org/10.1007/s10924-019-01379-1>.
- AASHTO MP 19-10, Standard Specification for Performance-Graded Asphalt Binder Using Multiple Stress Creep Recovery (MSCR) Test, ASTM International, West Conshohocken, PA, 2018, <https://doi.org/10.1520/D8239-18>.
- ASTM D6373-21a, Standard Specification for Performance-Graded Asphalt Binder, ASTM International, West Conshohocken, 2021, p. 1. –1.
- ASTM D70-18a, Standard Test Method For Density of Semi-Solid Asphalt Binder (Pycnometer Method), ASTM International, West Conshohocken, 2018, p. 1. –1.
- ASTM D4402/D4402M-15, Standard Test Method For Viscosity Determination of Asphalt at Elevated Temperatures Using a Rotational Viscometer, ASTM International, West Conshohocken, 2022, p. 1. –12022.
- ASTM D7175-08, Standard test method for determining the rheological properties of asphalt binder using a dynamic shear Rheometer. Standard Test Method For Determining the Rheological Properties of Asphalt Binder Using a Dynamic Shear Rheometer, ASTM International, West Conshohocken, 2008.
- M.J. Chinchillas-Chinchillas, et al., Evaluation of the mechanical properties, durability and drying shrinkage of the mortar reinforced with polyacrylonitrile microfibers, *Constr. Build. Mater.* 210 (2019) 32–39, <https://doi.org/10.1016/j.conbuildmat.2019.03.178>.
- M.J. Chinchillas-Chinchillas, et al., A new application of recycled-PET/PAN composite nanofibers to cement-based materials, *J. Clean. Prod.* 252 (2020), <https://doi.org/10.1016/j.jclepro.2019.119827>.
- AASHTO, AASHTO T 240. Standard Method of Test for Effect of Heat and Air on a Moving Film of Asphalt Binder (Rolling Thin-Film Oven Test), American Association of State Highway and Transportation Officials, 2013, pp. 1–11.
- T.W. Kennedy, et al., Report SHRP-A-410. Superior performing asphalt pavements (Superpave): the product of the SHRP asphalt research program. <https://www.trb.org/publications/shrp/SHRP-A-410.pdf>.
- ASTM, Standard Specification for Performance Graded Asphalt Binder, American Society of Testig Materials, West Conshohocken, PA, 2016, <https://doi.org/10.1520/D6373-16>.
- ASTM D6373, ASTM D6373 - 16 Standard Specification for Performance Graded Asphalt Binder, ASTM International, West Conshohocken, PA, 2016, <https://doi.org/10.1520/D6373-16>.
- AASHTO, ls. AASHTO M320-09. Performance-Graded Asphalt Binder, American Association of State Highway and Transportation Officia, 2009, pp. 1–11.
- AASHTO, AASHTO T315. Determining the Rheological Properties of Asphalt Binder Using a Dynamic Shear Rheometer, American Association of State Highway and Transportation Officials, 2010, pp. 1–32.
- V. Radhakrishnan, M.R. Sri, K.S. Reddy, Evaluation of asphalt binder rutting parameters, *Constr. Build. Mater.* 173 (2018) 298–307, <https://doi.org/10.1016/j.conbuildmat.2018.04.058>.
- R. Dongré, J. D'Angelo, Refinement of superpave high-temperature binder specification based on pavement performance in the accelerated loading facility, *Transp. Res. Rec.* (1829) (2003) 39–46, <https://doi.org/10.3141/1829-06>.
- R. Delgado, K. Nam, H. Bahia, Why do we need to change $G^*/\sin\delta$ and how? *Road Mater. Pavement Des.* 7 (1) (2006) 7–27, <https://doi.org/10.1080/14680629.2006.9690024>.
- J.A. D'Angelo, The relationship of the mscr test to rutting, *Road Mater. Pavement Des.* 10 (2009) 61–80, <https://doi.org/10.1080/14680629.2009.9690236>, September 2014.

- [45] ASTM D 2872, ASTM D 2872. Standard Test Method for Effect of Heat and Air on a Moving Film of Asphalt (Rolling Thin-Film Oven Test), American Society of Testig Materials, West Conshohocken, PA, 2019, <https://doi.org/10.1520/D2872-19>.
- [46] AASHTO TP70, AASHTO TP70. Multiple Stress Creep Recovery (MSCR) Test of Asphalt Binder Using a Dynamic Shear Rheometer (DSR), American Association of State Highway and Transportation Officials, 2012.
- [47] AASHTO TP 101-14. (2014). AASHTO TP 101-14. Estimating Damage Tolerance of Asphalt Binders Using the Linear Amplitude Sweep (pp. 1–7). https://www.asphaltpavement.org/uploads/documents/Engineering_ETGs/Binder_201409/Teymourpour_LAS%20Test_Binder%20Grading%20Specification%20and%20Field%20Validation.pdf.
- [48] A.K. Kuchiishi, J.P.B. Carvalho, I.S. Bessa, K.L. Vasconcelos, L.L.B. Bernucci, Effect of temperature on the fatigue behavior of asphalt binder, *Appl. Rheol.* 29 (1) (2019) 30–40, <https://doi.org/10.1515/ARH-2019-0004>.
- [49] R.F. Ribeiro, L.C. Pardini, N.P. Alves, C.A.R.B. Júnior, Thermal Stabilization study of polyacrylonitrile fiber obtained by extrusion, *Polimeros* 25 (6) (2015) 523–530, <https://doi.org/10.1590/0104-1428.1938>.
- [50] Q. Ouyang, L. Cheng, H. Wang, K. Li, Mechanism and kinetics of the stabilization reactions of itaconic acid-modified polyacrylonitrile, *Polym. Degrad. Stab.* 93 (8) (2008) 1415–1421, <https://doi.org/10.1016/j.polymdegradstab.2008.05.021>.
- [51] X. Yu, H.S. Park, Synthesis and characterization of electrospun PAN/2D MoS₂ composite nanofibers, *J. Ind. Eng. Chem.* 34 (2016) 61–65, <https://doi.org/10.1016/j.jiec.2015.10.030>.
- [52] Y. Priyadarshini, S. Maheshwari, A. Padmarekha, J.M. Krishnan, Effect of mixing and compaction temperature on dynamic modulus of modified binder bituminous mixtures, *Procedia Soc. Behav. Sci.* 104 (2013) 12–20, <https://doi.org/10.1016/j.sbspro.2013.11.093>.
- [53] Z.I. Qasim, A.H. Abed, K.A. Almomen, Evaluation of mixing and compaction temperatures (MCT) for modified asphalt binders using zero shear viscosity and Cross-Williamson model, *Case Stud. Constr. Mater.* 11 (2019) e00302, <https://doi.org/10.1016/j.cscm.2019.e00302>.
- [54] F. Safaei, C. Castorena, Temperature effects of linear amplitude sweep testing and analysis, *Transp. Res. Rec.* 2574 (2016) 92–100, <https://doi.org/10.3141/2574-10>.
- [55] K. Chen, H. Zhang, Y. Gu, S. Zhao, Microscopic action and rheological properties of reinforced modified asphalt with varying fiber content, *Case Stud. Constr. Mater.* 18 (2023) e01824, <https://doi.org/10.1016/j.cscm.2023.e01824>. November 2022.
- [56] A. Foroutan Mirhosseini, A. Kavussi, M.H. Jalal Kamali, M.M. Khabiri, A. Hassani, Evaluating fatigue behavior of asphalt binders and mixes containing Date Seed Ash, *J. Civ. Eng. Manag.* 23 (8) (2017) 1164–1175, <https://doi.org/10.3846/13923730.2017.1396560>.
- [57] H. Chen, H.U. Bahia, Modelling effects of aging on asphalt binder fatigue using complex modulus and the LAS test, *Int. J. Fatigue* 146 (2021), 106150, <https://doi.org/10.1016/j.ijfatigue.2021.106150>. January.
- [58] W. Cao, Y. Wang, C. Wang, Fatigue characterization of bio-modified asphalt binders under various laboratory aging conditions, *Constr. Build. Mater.* 208 (2019) 686–696, <https://doi.org/10.1016/j.conbuildmat.2019.03.069>.
- [59] P. Saha Chowdhury, S.L.A. Noojilla, M.A. Reddy, Evaluation of fatigue characteristics of asphalt mixtures using cracking tolerance index (CTIndex), *Constr. Build. Mater.* 342 (2022), 128030, <https://doi.org/10.1016/j.conbuildmat.2022.128030>. PB.
- [60] K.P. Biligiri, K. Kaloush, J. Uzan, Evaluation of asphalt mixtures' viscoelastic properties using phase angle relationships, *Int. J. Pavement Eng.* 11 (2) (2010) 143–152, <https://doi.org/10.1080/10298430903033354>.
- [61] Y. Ayala del Toro, P. Garnica Anguas, H. Delgado Alamilla, Efecto de la temperatura en la evaluación de la fatiga en ligantes asfálticos, *Infraestruct. Vial* 18 (31) (2016) 5–13, <https://doi.org/10.15517/iv.v18i31.27755>.
- [62] V. Maliar, Cohesion properties of bitumen of different structures, *Procedia Eng.* 134 (2016) 121–127, <https://doi.org/10.1016/j.proeng.2016.01.048>.
- [63] A.R. Azarhoosh, F.M. Nejad, A. Khodaii, The influence of cohesion and adhesion parameters on the fatigue life of hot mix asphalt, *J. Adhes.* 93 (13) (2017) 1048–1067, <https://doi.org/10.1080/00218464.2016.1201656>.